



AUGUST 16 2023

Time reversal imaging of complex sources in a three-dimensional environment using a spatial inverse filter

Adam D. Kingsley ; Andrew Basham; Brian E. Anderson 



J Acoust Soc Am 154, 1018–1027 (2023)

<https://doi.org/10.1121/10.0020664>



View
Online



Export
Citation

CrossMark

Related Content

The physics of knocking over LEGO minifigures with time reversal focused vibrations for use in a museum exhibit

J Acoust Soc Am (February 2022)

The physics of knocking over LEGO minifigures with time reversal focused vibrations

J Acoust Soc Am (October 2019)

Knocking over LEGO minifigures with time reversal focused vibrations: Understanding the physics and developing a museum demonstration

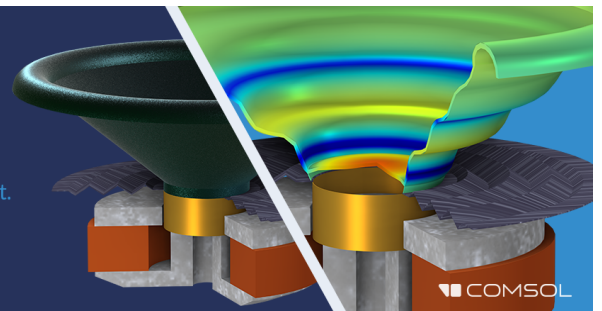
J Acoust Soc Am (October 2021)

22 August 2023 18:16:11

Take the Lead in Acoustics

The ability to account for coupled physics phenomena lets you predict, optimize, and virtually test a design under real-world conditions – even before a first prototype is built.

» Learn more about COMSOL Multiphysics®



Time reversal imaging of complex sources in a three-dimensional environment using a spatial inverse filter

Adam D. Kingsley,  Andrew Basham, and Brian E. Anderson^{a)} 

Acoustics Research Group, Department of Physics and Astronomy, Brigham Young University, Provo, Utah 84602, USA

ABSTRACT:

Time reversal focusing above an array of resonators creates subwavelength-sized features when compared to wavelengths in free space. Previous work has shown the ability to focus acoustic waves near the resonators with and without time reversal with an array placed coplanar with acoustic sources, principally using direct sound emissions. In this work, a two-dimensional array of resonators is studied with a full three-dimensional aperture of waves in a reverberation chamber and including significant reverberation within the time reversed emissions. The full impulse response is recorded, and the spatial inverse filter is used to produce a focus among the resonators. Additionally, images of complex sources are produced by extending the spatial inverse filter to create focal images, such as dipoles and quadrupoles. Although waves at oblique angles would be expected to degrade the focal quality, it is shown that complex focal images can still be achieved with super resolution fidelity when compared to free space wavelengths.

© 2023 Acoustical Society of America. <https://doi.org/10.1121/10.0020664>

(Received 20 January 2023; revised 21 July 2023; accepted 30 July 2023; published online 16 August 2023)

[Editor: Julien de Rosny]

Pages: 1018–1027

I. INTRODUCTION

A complex acoustic source can be described as a source with finite spatial extent and possibly nonuniform phase. In acoustics, the source can be rapidly imaged, e.g., by acoustic cameras.¹ However, determining the phase and amplitude distribution of such a source is complicated and becomes even more difficult when the dimensions of the source are subwavelength in scale and the distance to the detector is great. Furthermore, if the source is in a reverberant environment, then traditional beamforming techniques (e.g., as used by acoustic cameras) are greatly hindered by the inherent multiple scattering. Because of principles similar to the diffraction limit, recordings of waves in the far field of a source produce indistinguishable patterns.² Imaging is closely related to focusing of waves and, thus, the ability to focus a complex pattern is used to represent the ability to image a complex source. In other words, if a complex image can be created by distant sources, then a complex source can be imaged by distance receivers. The question of imaging a distant source then moves to the question of acoustic focusing at a distance.

Acoustic time reversal (TR) focusing is a well-studied topic^{3–6} and can be used for deliberate focusing of waves in many different contexts including medical ultrasound,^{7–11} non-destructive evaluation of structures using linear^{12–16} and nonlinear responses,^{17–24} nonlinear airborne sound,^{25–27} and some fun TR demonstrations with LEGO[®] (Billund, Denmark) minifigures.^{28,29} TR has also been used to image complex geophysical sources^{30–33} and aero-acoustic

sources^{34–37} by numerical backpropagation of the recorded waves. The simple process of TR begins with emitting a signal from a source and recording that signal with a receiver, or using a receiver to record the emissions from an unknown source. By time-reversing the recorded signal and broadcasting it from the receiver location, a focus is observed at the source location. Alternatively, if one has control over the source broadcast, then a chirp signal may be broadcast and a cross correlation of this chirp signal with the recorded response to this chirp signal yields the band limited impulse response (IR).^{38,39} This IR may be reversed in time and the broadcast of the time reversed IR (TRIR) yields delta-function like focusing of energy. This process of broadcasting the TRIR causes all frequencies to constructively interfere at a point in space and time. The TRIR may be broadcast from the original source and the focusing happens at the receiver, or the TRIR may be broadcast from the receiver location and the focus occurs back at the original source location. The temporal characteristics of the TR focus can be changed by convolving the TRIR with a desired signal and then broadcasting this modified TRIR. The new focal signal becomes the desired signal instead of the delta-function like response.

This reversal of the recordings is the simplest version of TR. When performed experimentally for laboratory testing, it is often convenient to broadcast the reversed recordings (i.e., TRIR) from the source locations instead of from the receiver locations. This method is sometimes called reciprocal TR⁵ because it depends on the reciprocity of the system to allow for an equivalent response between a pair of points, regardless of which point is the source and which is the

^{a)}Email: bea@byu.edu

receiver. Imaging a source can then be related to the ability to focus a spatiotemporal signal that represents the source. The ability to focus complex characteristics is then directly connected with the ability to image the complex characteristics of a source. Thus, if we can demonstrate in this paper that complex spatial patterns may be focused with TR, then this implies that unknown, complex sources may be imaged with similar techniques.

Sub-diffraction limited focusing has been the goal of many focusing methods.⁴⁰ TR has been shown to be capable of producing a focus much smaller than the diffraction limit would suggest in free space. This is performed by modifying the near-field of the focus using a source,⁴¹ absorbers,^{37,42,43} resonators,⁴⁴⁻⁴⁸ or scatterers.⁴⁹ Maznev and Wright² argued that because the diffraction limit was postulated for propagating waves, it does not apply to the near-field evanescent waves and thus sub-diffraction limited focus sizes are achieved if the free-space diffraction limit is used as the criterion. This can be understood by examining the boundary conditions. Near a boundary, the propagating waves must conform to match the boundary conditions. The boundary is under no constraints about resolution and so the waves, when close to a boundary, may have much higher spatial resolution than found in the free-space propagating wave.

When seeking to create a spatial focus, the impulse responses between each source and every point in the imaging area must be taken into consideration. A transfer function (\mathbf{H}) represents the frequency transform of the impulse response. At each frequency, \mathbf{H} is represented by a complex number, H_{SR} , and represents the response between source (\mathbf{S}) and receiver (\mathbf{R}) with both amplitude and phase. All the interactions between sources and receiver positions can then be represented with a matrix formulation:

$$\begin{bmatrix} H_{11} & \cdots & H_{n1} \\ \vdots & \ddots & \vdots \\ H_{1m} & \cdots & H_{nm} \end{bmatrix} \begin{bmatrix} S_1 \\ \vdots \\ S_n \end{bmatrix} = \begin{bmatrix} R_1 \\ \vdots \\ R_m \end{bmatrix}, \tag{1}$$

where n and m refer to the number of the source and receiver locations, respectively. The receiver locations are the various points in the imaging area. Although this equation only represents a single frequency, it describes a total response rather than the individual response represented by a single transfer function.

As written, Eq. (1) does not allow for producing a specified response. However, by inverting the transfer function matrix \mathbf{H} , a desired response vector \mathbf{R} can be used to discover the necessary source signals to produce such a response:

$$\begin{bmatrix} S_1 \\ \vdots \\ S_n \end{bmatrix} = \begin{bmatrix} H_{11} & \cdots & H_{n1} \\ \vdots & \ddots & \vdots \\ H_{1m} & \cdots & H_{nm} \end{bmatrix}^{-1} \begin{bmatrix} R_1 \\ \vdots \\ R_m \end{bmatrix}. \tag{2}$$

This spatial inverse method uses the inverse of \mathbf{H} to calculate the source vector \mathbf{S} and has been used in acoustics as

well as in electromagnetic propagation.^{50,51} A method of iteratively discovering the inverse transfer matrix has also been utilized in a similar TR experiment.⁴⁶ This problem is ill-posed and is often unstable. Taking the inverse of the transfer function can often lead to inverting small responses that are dominated by noise. The resulting inverse would then be dominated by these noisy signals. To solve this problem, a singular value decomposition is first performed producing a series of transfer matrices. Use of eigenmodes or a singular value decomposition have been used in acoustic TR in the past.^{52,53} Each transfer matrix can be represented as $\mathbf{H} = \mathbf{U}\mathbf{\Sigma}\mathbf{V}^\dagger$, where \mathbf{U} and \mathbf{V} contain a sequence of eigenmodes, † designates the conjugate-transpose operation, and $\mathbf{\Sigma}$ is a diagonal matrix whose elements consist of the corresponding eigenvalues. To invert this series of matrices requires taking the reciprocal of the elements (eigenvalues) in $\mathbf{\Sigma}$,

$$[\mathbf{U}\mathbf{\Sigma}\mathbf{V}^\dagger]^{-1} = [\mathbf{V}\mathbf{\Sigma}^{-1}\mathbf{U}^\dagger] = \mathbf{V} \begin{pmatrix} \begin{bmatrix} \frac{1}{\sigma_{11}} & 0 & \cdots & 0 \\ 0 & \frac{1}{\sigma_{22}} & \ddots & \vdots \\ \vdots & \ddots & \ddots & 0 \\ 0 & \cdots & 0 & \frac{1}{\sigma_{nn}} \end{bmatrix} \\ \mathbf{U}^\dagger \end{pmatrix}. \tag{3}$$

Because many of the eigenvalues are small, regularization is often applied. Before taking the reciprocal, a threshold for the eigenvalues is introduced and the eigenvalues above the threshold, l , are determined. After taking the inverse of $\mathbf{\Sigma}$, any elements originally below the threshold ($\sigma_{nn} < l$) are set to zero. In this way, a noise-filtered inverse of \mathbf{H} is calculated. The threshold can be determined empirically by using the quality of the results and repeating the process with different thresholds. For the experiments described in this paper, a threshold of 10% of the max was applied at each frequency to remove just the lowest eigenvalues. It is expected that improvement to this regularization would lead to an improved image using the resulting inverse matrix, but the main goal of this paper was not to attempt to optimize the inverse processing but rather show that the resonator array makes it possible to image complex sources.

It has not been previously shown whether complex sources can be focused with an array of resonators using TR. Interestingly, Orazbayev and Fleury⁵⁴ broadcast complex acoustic patterns of sound from an array of sources, whose radiated sound was then modulated by a “metalens”, or array of resonators before the sound reached an array of microphones. Deep learning was used with the microphone data to image the complex patterns and they showed that the metalens allowed better imaging of the patterns than when the metalens was not used. They did not use TR but it is an example where an array of resonators was beneficial in imaging complex acoustic source patterns.

The purpose of this paper is to show that complex sources may be imaged with sub-diffraction limited resolution using TR in the presence of an array of near-field resonators. This paper explores the ability of this spatial inverse filter method to produce complex images in the pressure field. An array of soda cans is used as was done in previous focusing work.^{46,55} This time, however, the array is in a reverberation chamber, and the full impulse response of the room [i.e., a three-dimensional (3-D) aperture] is utilized for focusing sound above this two-dimensional (2-D) array of resonators. In this paper, results are shown for an experimental setup where complex 2-D images are produced in the near-field of the resonators.

The work of Lemoult *et al.*⁴⁶ and of Maznev *et al.*⁵⁵ each restricted their experiments to principally include only the direct sound broadcasts from sources located in the plane of the array of resonators, either by time gating the signals recorded in the impulse response or by using an anechoic chamber. When the spatial focusing in the plane of an array is measured, waves that arrive from directions other than those in the plane of the array will have a larger wavelength projection in the plane than waves traveling in the plane (the same principle is involved in trace wavenumber matching for structural acoustics). Thus, waves arriving from directions other than those in plane may reduce the spatial resolution possible. This paper shows that it is still possible to attain super resolution while still utilizing waves that arrive out of the plane of the array of resonators, thus showing that it is not necessary to limit the impulse responses to the direct sound or require these experiments be done in an anechoic chamber.

II. EXPERIMENTAL SETUP

An array of soda cans constitutes an acoustic metamaterial, or phononic crystal, possessing properties that come from the arrangement and properties of the individual elements.⁴⁴ This array of soda cans has been previously shown

to produce focusing on the order of the size of the opening in a single soda can, although the resolution is actually limited by the discretization of the space, which is clearly the spacing between soda cans.^{46,55} Kingsley and Anderson⁴⁸ showed that each resonator (soda can) in the array is able to flip the phase of the incident sound, thereby providing a lower limit to the size of the sub-diffraction wavelengths to be the spacing between adjacent cans.

The current experiment places the 2-D metamaterial in a 3-D space to test the ability of the material to modify the waves and create images with high spatial frequency. In the reverberation chamber, some of the impinging waves come at oblique angles and do not interact with the whole array in the same way as coplanar waves. Prior work by Lemoult *et al.*⁴⁶ and Maznev *et al.*⁵⁵ principally or wholly utilized coplanar waves by placing the sources in the focusing plane. The received signals were then either time gated to include only the direct sound or an anechoic chamber or a relatively absorbent environment was utilized. This is similar to measuring a plane wave with an array of microphones. If the plane wave travels along the axis of the microphones, the measured wavelength is the true wavelength of the wave. However, if the plane wave is incident at an oblique angle to the microphone array, any incident wave manifests a wavelength across the array that is greater than the true wavelength of the wave.

The experimental setup consists of an array of soda cans (12 fl. oz.) held in a vertical plane as shown in Fig. 1(a). A 1 m² steel plate hangs on a vertical piece of medium density fiberboard. Each soda can has a small magnet glued to the underside that allows the cans to stay firmly in contact with the metal plate while also allowing the flexibility of other arrangements of the cans. Suspending the cans in the vertical plane allows the experiment to be moved away from the walls and floor where a spatial dependence to the focusing amplitude has been found.⁵⁶ The vertical plane was also convenient for the 2-D scanning system, which is positioned coplanar to the array with a microphone attached to the translation stage.

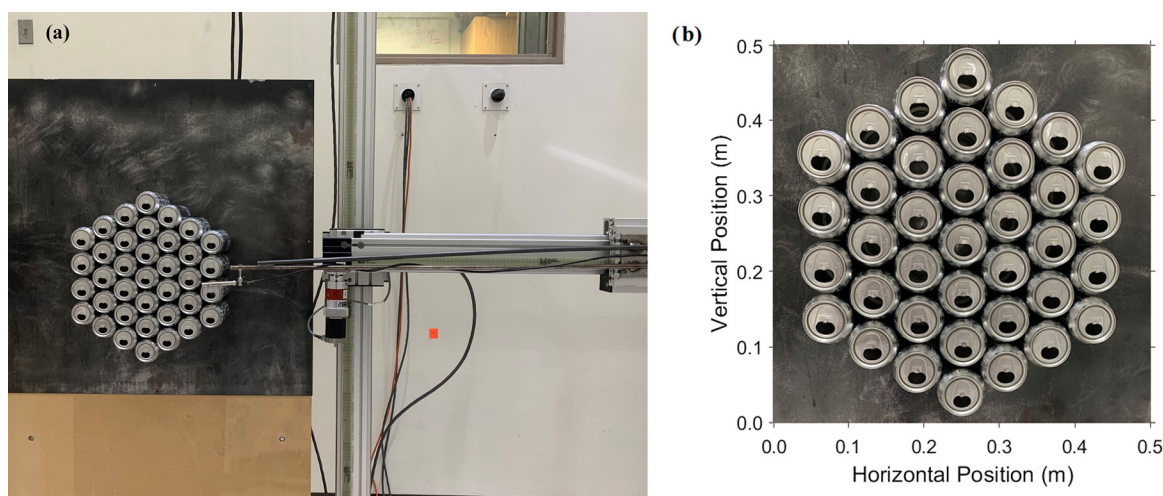


FIG. 1. (Color online) (a) Photograph of the experimental setup. (b) A hexagonal array of soda cans is mounted in the vertical plane and a 2-D scanning system is used to make measurements above the soda cans.

When moving over the array, the microphone is 1 cm above the soda cans. Eight Mackie (Bothell, WA) HR824mk2 loudspeakers are placed throughout the room roughly at the same height as the bottom of the resonator array constituting a horizontal plane that is perpendicular to the array of the cans (perpendicular to the focusing plane). The loudspeakers were oriented such that they were pointing away from the cans, towards the chamber walls to minimize the strength of the direct sound arrivals relative to the reverberant sound.³⁹ The whole setup is positioned within the large reverberation chamber at Brigham Young University. The chamber measures $4.96 \times 5.89 \times 6.98$ m with a total volume of 204 m^3 . The Schroeder frequency, a guideline given to approximately define the boundary between the modal dominated frequency range of a room and the frequency, above which, the field is assumed to be diffuse in the room, is 355 Hz. Custom LabVIEW software (ESTR), described in Ref. 57, is used along with a Spectrum Instrumentation (Grosshansdorf, Germany) MIMO system to control the loudspeakers, microphone, and scanning system.

The experimental procedure is similar to acoustic TR except, instead of simply reversing the impulse response, the spatial inverse filter described above [Eqs. (1)–(3)] is used to create the signals for the focusing step. The experiment results fed into the spatial inverse filter processing typically result in a signal-to-noise ratio of 35 dB; this is apparently a good enough signal-to-noise ratio to enable the spatial inverse filter to work as evidenced by the reasonable imaging results of the intended complex sources given in Sec. III. Alternatively, a technique such as iterative time reversal could be used,^{58–60} though we chose the spatial inverse filter for speed reasons. First, a series of chirp broadcasts are made from each source. The microphone is moved between sets of broadcasts to capture the response at each measurement position in the grid above the array of soda cans. Time invariance is assumed: multiple measurements are made by a single microphone placed at various positions and the measurements are assumed to imitate the simultaneous recording of microphones at all of those various positions. A swept sine wave (chirp) is used because it generates near uniform amplitude over a range of frequencies, which results in a high signal-to-noise measurement of the impulse response for the bandwidth.^{38,39} For this experiment, a grid of 51×51 points was used with a spacing of 1 cm. Since each can has an opening of just over 1 cm^2 , this ensures that a measurement point is over some portion of each can's opening. Figure 1(b) shows the measurement area, as well as the position of the cans, relative to the measurement area.

The chirp had a bandwidth of 300–425 Hz. This includes frequencies below the Schroeder frequency, but a diffuse field is not strictly required for TR. The existence of strong modes can skew the spatial distribution of the focusing some, possibly resulting in stronger than usual spatial side lobes in the focusing. Soda cans with a higher Helmholtz resonance frequency could have been used to avoid this issue. Reverberation chambers have relatively high Schroeder frequencies due to their lack of damping.

The majority of the frequency content used in the super-resolution focusing ended up existing above the 355 Hz Schroeder frequency. This frequency range was intentionally chosen to fall below the Helmholtz resonance frequency of a single can since others have shown that modes with small effective wavelengths exist below this resonance and tighter spatial focusing may thus be obtained below, as opposed to above, this resonance frequency.^{46,55}

By cross correlating the response with the chirp signals, an impulse response is obtained between each source and receiver position. A Fourier transform of these impulse responses yields a series of transfer matrices, one for each frequency. Using the inverse of an individual transfer matrix \mathbf{H} , the necessary signal \mathbf{S} , can be calculated from a desired response \mathbf{R} , for a single frequency. This spatial inverse method was performed by solving Eq. (2) for each frequency and producing spectra for each source. Due to the attenuation of the array, an upper frequency of 410 Hz was used during this step, leading to an effective bandwidth of 300–410 Hz. An inverse Fourier transform then produces a set of eight time signals, which are broadcast into the system and generate a focus above the array. Figure 2 shows the magnitude of the spectrum for the chirp, an example spectrum of an impulse response, an example spectrum produced by the spatial inverse filter, and an example resulting focus spectrum. The drop in amplitude as the frequency approaches the resonance of a single can (approximately 400 Hz) is seen in the impulse response spectrum. This attenuation near resonance is expected by previous research into reflection by single resonators but also by the resonator arrays constructed previously.^{46,55} Additional related research on the subject of hybridization band gaps and negative index metamaterials have explored this attenuation.^{61–66}

It is worth noting that the full width at half maximum (FWHM) for the various resonances of the soda can array, visible as the peaks in Fig. 2, are on the order of 1 Hz. In room acoustics theory, the FWHM for a room mode is inversely proportional to the reverberation time, RT_{60} , of the room as $FWHM = 2.2/RT_{60}$, which means that the effective reverberation time of the modes of the soda can array is about 2.2 s. The measured reverberation time of the reverberation chamber is about 4–5 s in this frequency range (with the uncertainty depending on the measurement location). This means that the room generally has less damping than the soda cans, but perhaps only different by a factor of 2.

III. RESULTS

The results from a series of experiments are described in this section. The results utilize the process described above with several different specified response patterns. The rectangular grid above the soda cans consists of 2601 points. This grid was trimmed down to a hexagonal area which represents the measurement surface made above the resonator array. For the 1392 locations above the resonator array, the pressures at the focal time compose the desired image \mathbf{R} . The experiments conducted in this paper only used a few

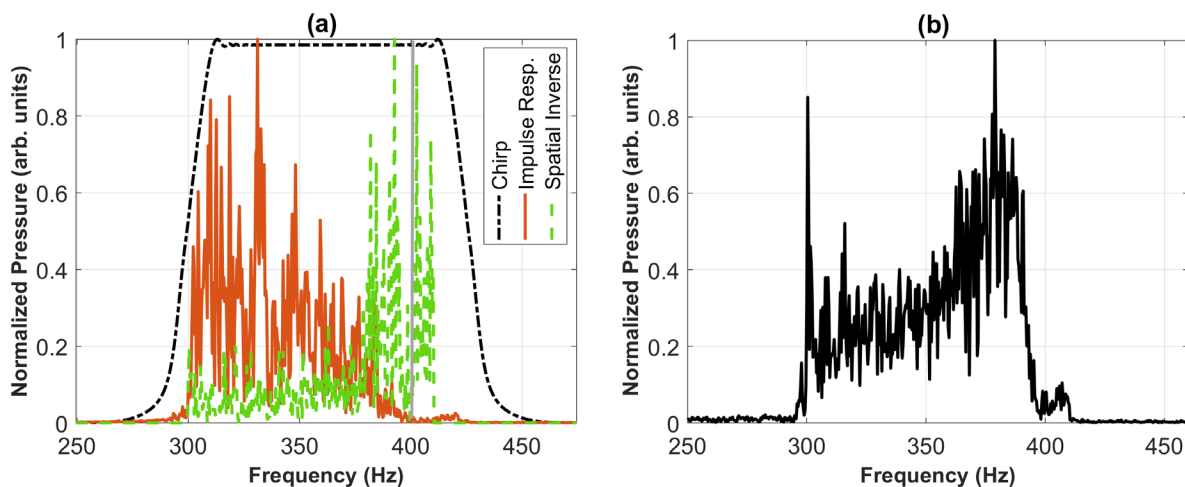


FIG. 2. (Color online) (a) Spectra for the forward signal (black, dotted-dashed), the calculated impulse response (red, solid), and the derived signal to create a point focus using a spatial inverse filter (green, dashed). (b) The spectrum at the resulting focus. The approximate resonance frequency of a single resonator is at 400 Hz.

points that were set to nonzero values to define the locations of the poles of each source. Although the image is 2-D, Eq. (2) uses a 1-D vector of sources and receiver positions, regardless of their relative positions. This vectorized image, \mathbf{R} , was then combined with each frequency of the transfer matrix, \mathbf{H} , one by one, to obtain the spectra of the source signals, \mathbf{S} . These spectra were converted to time waveforms, imported into ESTR, and broadcast simultaneously from all loudspeakers.

A. Monopole focusing

The first and most simple focusing is that of a monopole, point focus. By setting a single point of \mathbf{R} to be one, and all other points to be zero, the sharpest focusing can be measured. Monopole focusing at two different positions is shown in Fig. 3 at an instant in time when the focal amplitude is the largest (focal time). Also shown is the case when cans are not present. Without the cans present, the microphone scan density did not need to be as fine since the focal width was much wider. A linear interpolation between measurement points was done so that the FWHM determination

utilized the same spatial resolution as the finer density spatial scans. The linear interpolation tends to bias the FWHM low. Positions above individual soda cans were chosen as targets.

It is evident from Fig. 3 that the spatial inverse filter can produce a focus that is much smaller in spatial extent than without the cans present. In the case of no resonators, the spatial inverse filter does not produce a maximum at the focal location. This error in the location of the focus without cans may be caused by a nonideal threshold applied to the Singular Value Decomposition (SVD) process. This threshold is responsible for filtering out noise before the inverse is calculated. Perhaps the more likely reason for the maximum not being at the focal location is that the room is being driven at frequencies below the Schroeder frequency, where some individual room modes may be strongly contributing to the spatial distribution of the focusing. Regardless of the shift in peak location, the important point here is that the spatial extent of the focusing of a monopole without cans present is much wider than with the cans present.

Although using the spatial inverse filter couples the responses of the sources, the frequencies are still

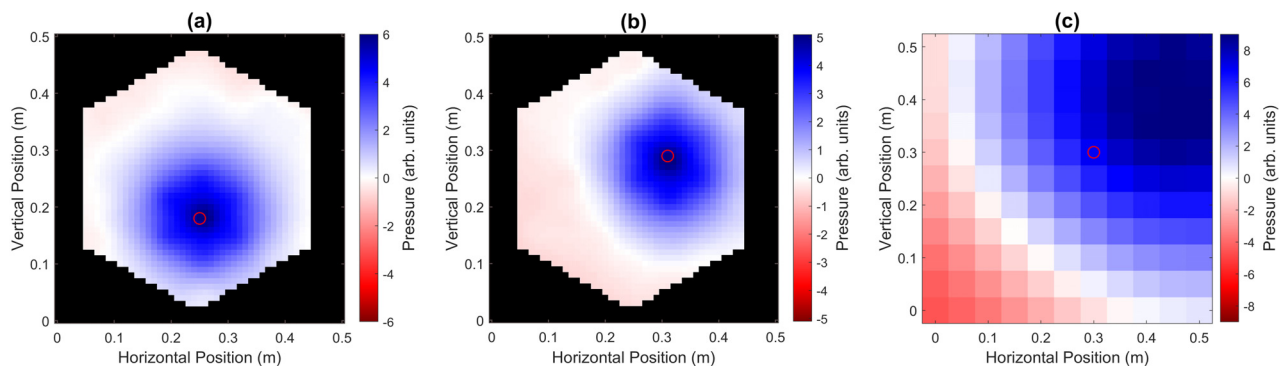


FIG. 3. (Color online) Spatial plots of the pressure amplitude over the array for the monopole case at focal time. Blue represents high pressure and red represents low (or negative) pressure. A red circle marks the target position. (a) Focus at the can just below center. (b) Focus at the can above and to the right of center. (c) A case without resonators with the focus location shown with a red circle.

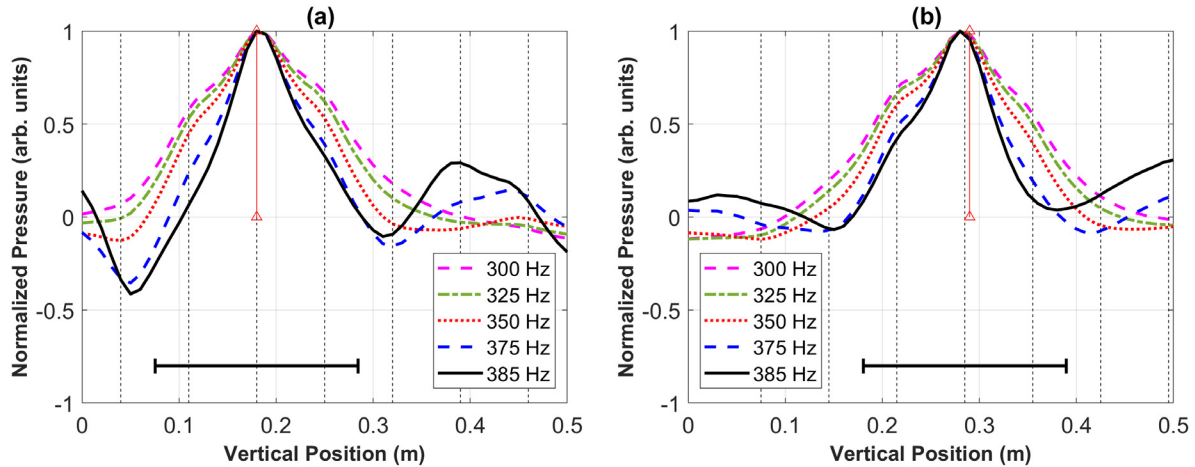


FIG. 4. (Color online) Normalized pressure above an array of soda cans at focal time. (a) and (b) Results obtained for two different focusing locations [corresponding to Figs. 3(a) and 3(b)]. The target focus location is shown with a vertical line and a red arrow. Several bandwidths are shown with the lower limit in the legend and a constant upper limit of 410 Hz. A quarter wavelength at 410 Hz is marked, for scale, with a black horizontal line. As the passband becomes smaller, the focus becomes tighter. Black dashed vertical lines denote the locations of can openings.

independent variables. Because the frequencies are independent, a target image can be achieved more easily with some frequencies than others. Bringing together the contributions of the many frequencies may lend more total power to frequencies for which the target image is not well reproduced. For the array of soda cans, the dispersion relation does not follow a linear function of frequency and yields much smaller wavelengths than in free space and has been explored previously.^{47,55} With the assumption that high-resolution images are more able to be generated with higher frequencies, the focus above the cans was filtered with progressively smaller bandwidth (while maintaining the same upper frequency cutoff and using that same upper frequency to define the resolution in each case). We selected eigenvalues on a frequency by frequency basis, but they could have been selected by choosing the best eigenvalues seen over multiple frequencies, thereby coupling the thresholds. With a reduced bandwidth the focus becomes tighter, suggesting that coupling the thresholds between frequencies may have the advantage of increasing the sharpness of the focus. Figure 4 shows the spatial extent of the focusing when using a bandpass filter with the lower frequency marked in the legend. As the lower passband frequency increases, the focus becomes tighter (and is always better with resonators present than without).

The results in Fig. 4 are further analyzed by considering the FWHM lengths in Table I. These values are taken from

TABLE I. Full width at half-maximum (FWHM) values of the focal pressure for the bandwidths used in Fig. 2, with λ as the free field wavelength at 410 Hz. Positions 1 and 2 mentioned correspond to the two shown in Figs. 3(a) and 3(b).

Lower passband frequency	300 Hz	325 Hz	350 Hz	375 Hz	385 Hz
Position 1 FWHM	0.202 λ	0.188 λ	0.164 λ	0.115 λ	0.113 λ
Position 2 FWHM	0.204 λ	0.193 λ	0.170 λ	0.128 λ	0.108 λ
No cans FWHM	0.596 λ	0.576 λ	0.570 λ	0.572 λ	0.564 λ

the graphs in Fig. 4 but written in terms of the free-space wavelength in air of the highest frequency in the bandwidth (410 Hz). The size of the focusing at the two different target focal positions is similar and always much better than without the resonators present. As expected, the values also show that the higher frequencies are much more capable at producing a sharp focus when compared to the case without resonators. For the narrowest filter results shown, the bandwidth is only 25 Hz; this case is still capable of focusing to a target position and produces a focus at a location five times smaller than without the cans present. This result is impressive because in the limit that the bandwidth narrows to a single frequency, the waveform becomes a sine wave with no distinct focus. So, although the array of soda cans is only 2-D and many waves may come from oblique angles to the array, the array is still capable of interacting with the coplanar waves sufficiently to cause a high spatial frequency in the resulting focus. This work lends confidence to the ability of a 2-D acoustic metamaterial to improve imaging, even in a 3-D space. For future applications, it is important to understand that these results were obtained when the loudspeakers are in a plane that is perpendicular to the plane of the soda cans and that the multiple scattering (reverberation) exploited by the TR process tends to provide incident waves from all directions.

B. Dipole wave field

The next imaging case considered was the focusing of a dipole wave field and its orientation. To generate a dipole focus, two points of \mathbf{R} were chosen to have nonzero values of +1 and -1. Two dipoles, one in the vertical and one in the horizontal plane, were focused. The resulting spatial maps are shown in Fig. 5. Although the vertical dipole is well aligned with the vertical axis, the horizontal dipole suffers from some angular uncertainty and looks more like it is focusing diagonally. This difference may have to do with the symmetries in the array of cans. For closer examination,

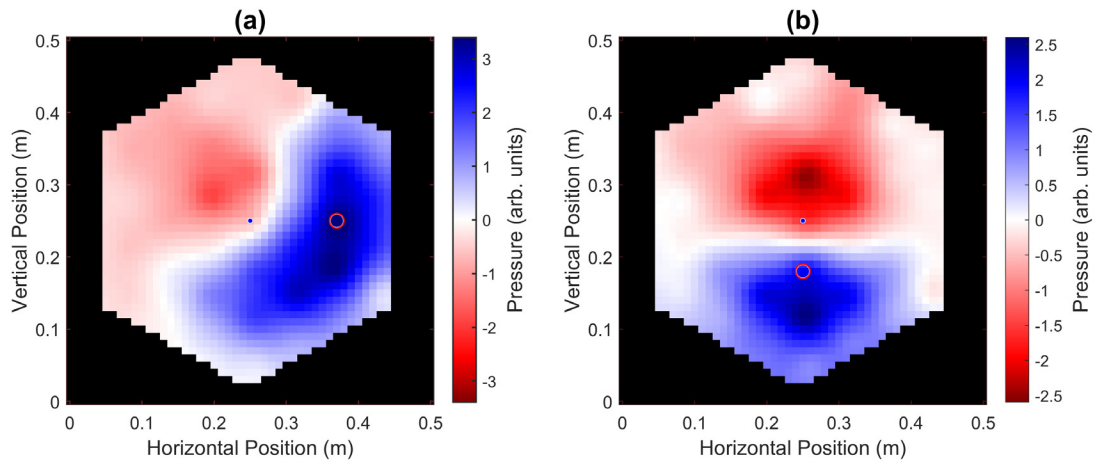


FIG. 5. (Color online) The spatial extent of a horizontal (left) and vertical (right) dipole at focal time. Blue represents high pressure and red represents low pressure. A red circle marks the target positive pole. The smaller blue dot marks the target negative pole.

a horizontal line scan through the two poles of Fig. 5(a) is plotted in Fig. 6(a) and a vertical line scan through the two poles of Fig. 5(b) is plotted in Fig. 6(b). The horizontal dipole has an asymmetric shape with a broad and lower amplitude negative pole and a more sharply defined positive pole with a higher amplitude. The spatial map, however, shows that the orientation seems to be the source of the error. There are possible reasons for this result. A strong mode may be limiting the resolution of this dipole. Also, a position closer to the edge of the array was used for targeting. Positions close to the edge should exhibit properties somewhere between that of central portion of the array (where tighter spatial focusing is possible) and free space (where the spatial focusing is diffraction limited). Another feature shown in Fig. 6 are bumps above each resonator. These bumps were predicted by a previous model of a 1-D array using an equivalent circuit approach⁴⁷ and show a strong near-field interaction with the resonators.

C. Quadrupoles

Two different types of quadrupoles were attempted. A vertically oriented longitudinal quadrupole and a lateral quadrupole. Similar to the dipole cases, several values of \mathbf{R} were set to nonzero values. As shown in Fig. 7, for the vertical longitudinal quadrupole, the positive poles were collocated, and the resulting target amplitudes were $[-0.5 \ 1 \ -0.5]$ within the \mathbf{R} vector. The lateral quadrupole did not have the poles placed over cans but instead were placed nearly centered between the cans in a square arrangement. Since the four poles could not all be placed over can openings, it seemed to make sense to place none of them over openings to avoid skewing the results by unequally favoring the focusing of each pole. The patterns for both quadrupoles are in very good agreement with the expected pressure patterns of these classic source arrangements. Figure 8 shows a plot of the 1-D pressure along the vertical axis of the longitudinal quadrupole. A quadrupole was created but the position of the poles

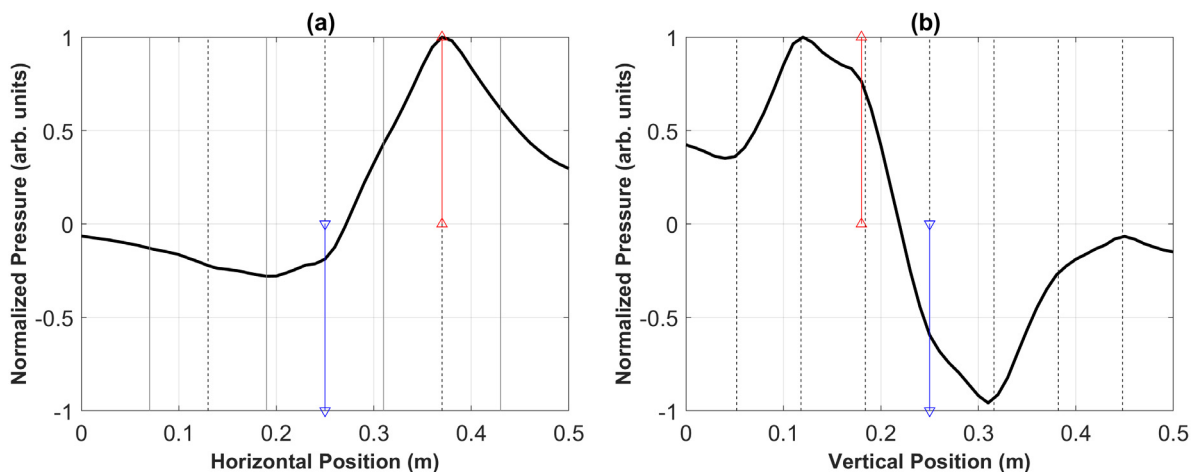


FIG. 6. (Color online) Normalized pressure values along the axis of the horizontal (left) and vertical (right) dipoles at focal time. The target positive pole is shown with a vertical line and a red arrow (pointing up) and the target negative pole is shown with a vertical line and a blue arrow (pointing down). The positions of cans along the axis are shown with dashed vertical lines. The horizontal dipole has columns of cans that are in rows just above or below and thus staggered relative to the cans lying along the horizontal dipole line; these are marked with a solid gray line.

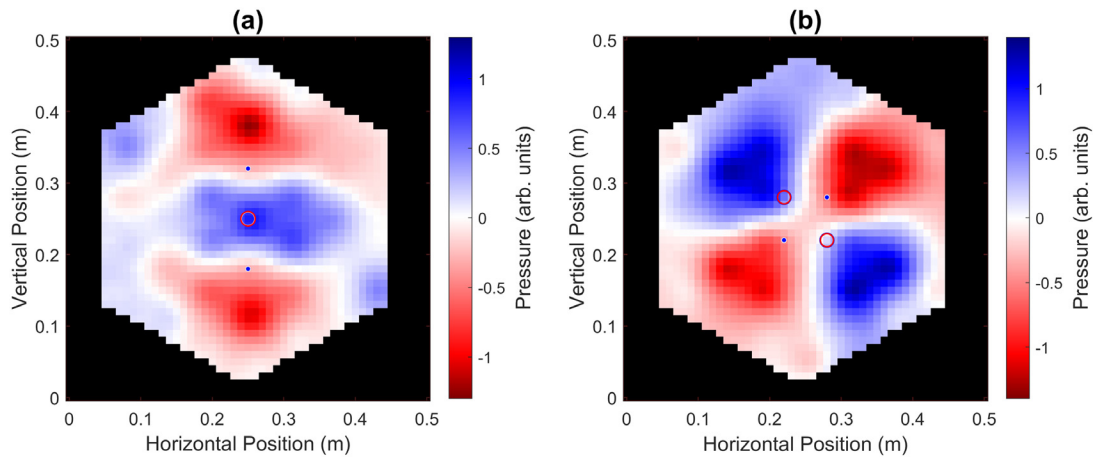


FIG. 7. (Color online) Pressure amplitudes at focal time for (a) vertically oriented longitudinal and (b) lateral quadrupole. These patterns show nodal lines and spatial extent that is much smaller than could be reproduced without the resonators. Blue represents high pressure and red represents low pressure. Red circles mark target positive poles. The smaller red dots mark target negative poles.

does not exactly match that of the target pattern. When comparing the quadrupole results with the cans present to the corresponding results without the resonators present (spatial inverse filter used in both cases and pole locations were the same), the resulting pressure fields show faint signs of creating the target patterns—but not all of the poles are captured in the resulting image. Whereas with the resonators present, the spatial extent of the patterns is much tighter.

D. Complex pattern

The last target pattern was a much more complex pattern. An attempt was made to obtain a “Y” pattern (a simplified version of the Brigham Young University logo). The R vector contains 19 nonzero values with seven values set to +1 and 12 values set to -1. Figure 9 shows the result of this attempt. The signals here were filtered with a bandpass from

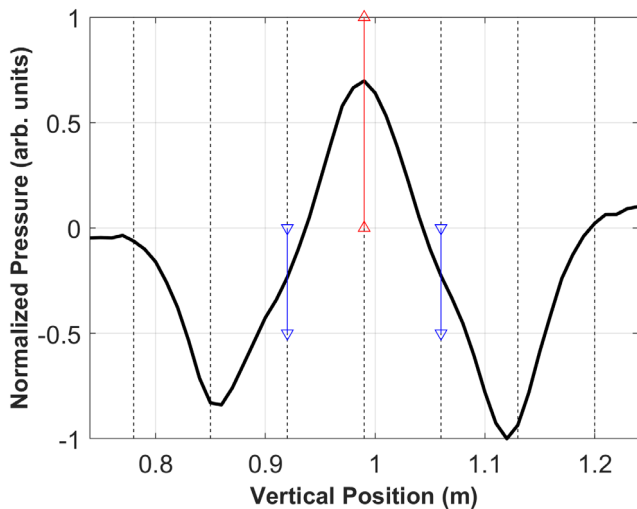


FIG. 8. (Color online) One-dimensional plot of the normalized pressure of the longitudinal quadrupole along the vertical axis at focal time. The positions of the positive and negative poles are denoted by vertical lines with red and blue colored arrows (positive arrow pointing up and negative arrow pointing down), respectively.

375 to 410 Hz. The resulting pattern does indeed resemble a “Y” but suffers from resolution limitations near the arms of the “Y”. There appears to be a positive pressure hexagon shape around the outside perimeter that distorts the intended image, most likely due to fringe effects. Figure 9 also shows a cropped image and modified color map meant to empirically enhance the image of the “Y”.

IV. CONCLUSION

As evidenced by the spatial results or imaging of complex sources shown in this paper, a 2-D array of resonators (constituting a resonant acoustic metamaterial) is capable of modifying near-field pressure in a 3-D environment. This capability to recreate complex imaging fields, including orientation, means that the ability to image a complex source located near a resonant material could be improved beyond the diffraction limit of free-space waves. In effect, the material can extend the size of the source, relative to a wavelength, in a similar fashion to a lens, and enable far-field imaging of sub-wavelength features. Limitations on the ability to create any arbitrary image could possibly occur due to the arrangement of sources or the geometry of the setup. Specifically, knowledge of the impulse responses above the resonators is necessary to create the images seen in this work using a spatial inverse filter. Other techniques besides the spatial inverse filter may prove to work better and the spatial inverse filter process used here may not be ideal, but the method used here was deemed sufficient to show that complex sources may be imaged with the resonator array present.

This work is a natural extension of previous work with acoustic metamaterials and especially arrays of resonators. This study has shown subwavelength focusing is possible because the wavelengths above the array are much smaller than in free space. The results confirm that using a simultaneous solution, such as inverting the transfer matrix to obtain a spatial inverse filter, is a viable method for producing high-resolution images from a distance. Evidence has

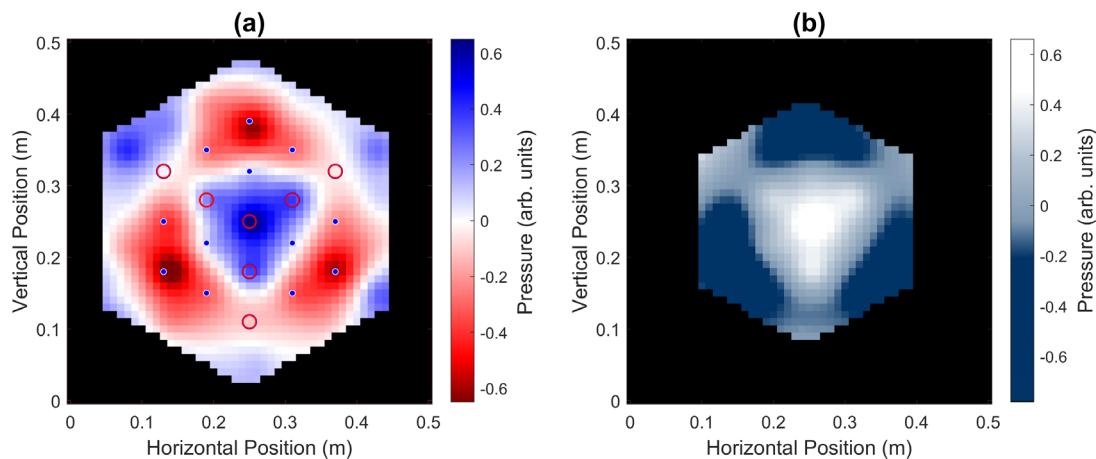


FIG. 9. (Color online) (a) A complex “Y” target pattern is obtained over resonators at focal time. Blue represents high pressure and red represents low pressure. Red circles mark target positive poles. The smaller red dots mark target negative poles. (b) By reducing the image area and adjusting the color scale, an improved version of the “Y” is easier to see (right).

been given that the full impulse response, including reflections arriving from all directions within the room and scatterers, does not meaningfully impair the ability to produce sub-diffraction limited images. Although the spatial inverse filter solves for the contributions from all of the sources at a single frequency, some frequencies have higher spatial frequencies above the cans and manually filtering the results or coupling the thresholds, can yield even tighter focusing.

ACKNOWLEDGMENTS

Funding was provided by Los Alamos National Laboratory, subcontract number 527136, under the technology maturation program. Additional support was provided by the BYU College of Physical and Mathematical Sciences.

¹B. Zimmermann and C. Studer, “FPGA-based real-time acoustic camera prototype,” in *Proceedings of 2010 IEEE International Symposium on Circuits and Systems*, Salt Lake City, UT (American Rock Mechanics Association, Alexandria, VA, 2010), pp. 1419–1422.
²A. A. Maznev and O. B. Wright, “Upholding the diffraction limit in the focusing of light and sound,” *Wave Motion* **68**, 182–189 (2017).
³A. Parvulescu and C. S. Clay, “Reproducibility of signal transmissions in the ocean,” *Radio Electron. Eng. UK*, **29**(4), 223–228 (1965).
⁴M. Fink, “Time reversed acoustics,” *Phys. Today* **50**(3), 34–40 (1997).
⁵B. E. Anderson, M. Griffa, C. Larmat, T. J. Ulrich, and P. A. Johnson, “Time reversal,” *Acoust. Today* **4**(1), 5–16 (2008).
⁶C. S. Clay and B. E. Anderson, “Matched signals: The beginnings of time reversal,” *Proc. Mtgs. Acoust.* **12**, 055001 (2011).
⁷J.-L. Thomas, F. Wu, and M. Fink, “Time reversal focusing applied to lithotripsy,” *Ultrason. Imaging* **18**(2), 106–121 (1996).
⁸M. Tanter, J.-L. Thomas, and M. Fink, “Focusing and steering through absorbing and aberrating layers: Application to ultrasonic propagation through the skull,” *J. Acoust. Soc. Am.* **103**(5), 2403–2410 (1998).
⁹G. Montaldo, P. Roux, A. Derode, C. Negreira, and M. Fink, “Ultrasound shock wave generator with one-bit time reversal in a dispersive medium, application to lithotripsy,” *Appl. Phys. Lett.* **80**(5), 897–899 (2002).
¹⁰M. Fink, G. Montaldo, and M. Tanter, “Time-reversal acoustics in biomedical engineering,” *Annu. Rev. Biomed. Eng.* **5**, 465–497 (2003).
¹¹S. Dos Santos and Z. Prevorovsky, “Imaging of human tooth using ultrasound-based chirp-coded nonlinear time reversal acoustics,” *Ultrasonics* **51**(6), 667–674 (2011).

¹²C. Prada and M. Fink, “Separation of interfering acoustic scattered signals using the invariant of the time-reversal operator. Application to Lamb waves characterization,” *J. Acoust. Soc. Am.* **104**, 801–807 (1998).
¹³E. Kerbrat, R. K. Ing, C. Prada, D. Cassereau, and M. Fink, “The D.O.R.T. method applied to detection and imaging in plates using Lamb waves,” *AIP Conf. Proc.* **557**, 934–940 (2001).
¹⁴E. Kerbrat, C. Prada, D. Cassereau, and M. Fink, “Ultrasonic nondestructive testing of scattering media using the decomposition of the time reversal operator,” *IEEE Trans. Ultrason. Ferroelect. Freq. Contr.* **49**, 1103–1113 (2002).
¹⁵C. Prada, E. Kerbrat, D. Cassereau, and M. Fink, “Time reversal techniques in ultrasonic nondestructive testing of scattering media,” *Inverse. Probl.* **18**, 1761–1773 (2002).
¹⁶B. E. Anderson, M. Griffa, P.-Y. L. Bas, T. J. Ulrich, and P. A. Johnson, “Experimental implementation of reverse time migration for nondestructive evaluation applications,” *J. Acoust. Soc. Am.* **129**(1), EL8–EL14 (2011).
¹⁷M. A. Jaimes and R. Snieder, “Spatio-temporal resolution improvement via weighted time-reversal,” *Wave Motion* **106**, 102803 (2021).
¹⁸T. J. Ulrich, A. M. Sutin, T. Claytor, P. Papin, P.-Y. Le Bas, and J. A. TenCate, “The time reversed elastic nonlinearity diagnostic applied to evaluation of diffusion bonds,” *Appl. Phys. Lett.* **93**(15), 151914 (2008).
¹⁹B. E. Anderson, M. Griffa, T. J. Ulrich, P.-Y. L. Bas, R. A. Guyer, and P. A. Johnson, “Crack localization and characterization in solid media using time reversal techniques,” in *Proceedings of the 44th U.S. Rock Mechanics Symposium and 5th U.S.-Canada Rock Mechanics Symposium*, paper No. ARMA-10-154 (2010).
²⁰P.-Y. L. Bas, M. C. Remillieux, L. Pieczonka, J. A. Ten Cate, B. E. Anderson, and T. J. Ulrich, “Damage imaging in a laminated composite plate using an air-coupled time reversal mirror,” *Appl. Phys. Lett.* **107**(18), 184102 (2015).
²¹B. E. Anderson, L. Pieczonka, M. C. Remillieux, T. J. Ulrich, and P.-Y. Le Bas, “Stress corrosion crack depth investigation using the time reversed elastic nonlinearity diagnostic,” *J. Acoust. Soc. Am.* **141**(1), EL76–EL81 (2017).
²²B. E. Anderson, M. C. Remillieux, P.-Y. L. Bas, and T. J. Ulrich, “Time reversal techniques,” in *Nonlinear Acoustic Techniques for Nondestructive Evaluation*, 1st ed., edited by T. Kundu (Springer and Acoustical Society of America, 2018), pp. 547–581.
²³S. M. Young, B. E. Anderson, S. M. Hogg, P.-Y. L. Bas, and M. C. Remillieux, “Nonlinearity from stress corrosion cracking as a function of chloride exposure time using the time reversed elastic nonlinearity diagnostic,” *J. Acoust. Soc. Am.* **145**(1), 382–391 (2019).
²⁴S. M. Young, B. E. Anderson, M. L. Willardson, P. E. Simpson, and P.-Y. Le Bas, “A comparison of impulse response modification techniques for time reversal with application to crack detection,” *J. Acoust. Soc. Am.* **145**(5), 3195–3207 (2019).
²⁵M. L. Willardson, B. E. Anderson, S. M. Young, M. H. Denison, and B. D. Patchett, “Time reversal focusing of high amplitude sound in a reverberation chamber,” *J. Acoust. Soc. Am.* **143**(2), 696–705 (2018).

- ²⁶C. B. Wallace and B. E. Anderson, “High-amplitude time reversal focusing of airborne ultrasound to generate a focused nonlinear difference frequency,” *J. Acoust. Soc. Am.* **150**(2), 1411–1423 (2021).
- ²⁷B. D. Patchett and B. E. Anderson, “Nonlinear characteristics of high amplitude focusing using time reversal in a reverberation chamber,” *J. Acoust. Soc. Am.* **151**(6), 3603–3614 (2022).
- ²⁸C. Heaton, B. E. Anderson, and S. M. Young, “Time reversal focusing of elastic waves in plates for an educational demonstration,” *J. Acoust. Soc. Am.* **141**, 1084–1092 (2017).
- ²⁹L. A. Barnes, B. E. Anderson, P.-Y. Le Bas, A. D. Kingsley, A. C. Brown, and H. R. Thomsen, “The physics of knocking over LEGO mini-figures with time reversal focused vibrations,” *J. Acoust. Soc. Am.* **151**(2), 738–751 (2022).
- ³⁰C. Larmat, J.-P. Montagner, M. Fink, Y. Capdeville, A. Tourin, and E. Clévéde, “Time-reversal imaging of seismic sources and application to the great Sumatra earthquake,” *Geophys. Res. Lett.* **33**, L19312, <https://doi.org/10.1029/2006GL026336> (2006).
- ³¹C. Larmat, J. Tromp, Q. Liu, and J.-P. Montagner, “Time reversal location of glacial earthquakes,” *J. Geophys. Res.* **113**(B9), B09314, <https://doi.org/10.1029/2008JB005607> (2008).
- ³²C. Larmat, R. A. Guyer, and P. A. Johnson, “Tremor source location using time-reversal: Selecting the appropriate imaging field,” *Geophys. Res. Lett.* **36**(22), L22304, <https://doi.org/10.1029/2009GL040099> (2009).
- ³³C. S. Larmat, R. A. Guyer, and P. A. Johnson, “Time-reversal methods in geophysics,” *Phys. Today* **63**(8), 31–35 (2010).
- ³⁴I. Rakotoarisoa, J. Fischer, V. Valeau, D. Marx, C. Prax, and L.-E. Brizzi, “Time-domain delay and sum beamforming for time-reversal detection of intermittent acoustic sources in flows,” *J. Acoust. Soc. Am.* **136**(5), 2675–2686 (2014).
- ³⁵A. Mimani, Z. Prime, C. J. Doolan, and P. R. Medwell, “A sponge-layer damping technique for aeroacoustic time-reversal,” *J. Sound Vib.* **342**, 124–151 (2015).
- ³⁶A. Mimani, Z. Prime, D. J. Moreau, and C. J. Doolan, “An experimental application of aeroacoustic time-reversal to the Aeolian tone,” *J. Acoust. Soc. Am.* **139**(2), 740–763 (2016).
- ³⁷A. Mimani, “A point-like enhanced resolution of experimental Aeolian tone using an iterative point-time-reversal-sponge-layer damping technique,” *Mech. Syst. Signal. Process.* **151**, 107411 (2021).
- ³⁸B. Van Damme, K. Van Den Abeele, Y. Li, and O. Bou Matar, “Time reversed acoustics techniques for elastic imaging in reverberant and non-reverberant media: An experimental study of the chaotic cavity transducer concept,” *J. Appl. Phys.* **109**(10), 104910 (2011).
- ³⁹B. E. Anderson, M. Clemens, and M. L. Willardson, “The effect of transducer directionality on time reversal focusing,” *J. Acoust. Soc. Am.* **142**(1), EL95–EL101 (2017).
- ⁴⁰F. Ma, Z. Huang, C. Liu, and J. H. Wu, “Acoustic focusing and imaging via phononic crystal and acoustic metamaterials,” *J. Appl. Phys.* **131**, 011103 (2022).
- ⁴¹J. de Rosny and M. Fink, “Publisher’s Note Overcoming the diffraction limit in wave physics using a time-reversal mirror and a novel acoustic sink [Phys. Rev. Lett. **89**(12), 124301 (2002)],” *Phys. Rev. Lett.* **89**(12), 219901 (2002).
- ⁴²G. Ma, X. Fan, F. Ma, J. de Rosny, P. Sheng, and M. Fink, “Towards anti-casual Green’s function for three-dimensional sub-diffraction focusing,” *Nat. Phys.* **14**(6), 608–612 (2018).
- ⁴³F. Ma, J. Chen, J. Wu, and H. Jia, “Realizing broadband sub-wavelength focusing and a high intensity enhancement with a space-time synergetic modulated acoustic prison,” *J. Mater. Chem. C* **8**, 9511–9519 (2020).
- ⁴⁴G. Lerosey, J. de Rosny, A. Tourin, and M. Fink, “Focusing beyond the diffraction limit with far-field time reversal,” *Science* **315**(5815), 1120–1122 (2007).
- ⁴⁵S. G. Conti, P. Roux, and W. A. Kuperman, “Near-field time-reversal amplification,” *J. Acoust. Soc. Am.* **121**(6), 3602–3606 (2007).
- ⁴⁶F. Lemoult, M. Fink, and G. Lerosey, “Acoustic resonators for far-field control of sound on a subwavelength scale,” *Phys. Rev. Lett.* **107**(6), 064301 (2011).
- ⁴⁷A. D. Kingsley, B. E. Anderson, and T. J. Ulrich, “Super-resolution within a one-dimensional phononic crystal of resonators using time reversal in an equivalent circuit model,” *J. Acoust. Soc. Am.* **152**(3), 1263–1271 (2022).
- ⁴⁸A. D. Kingsley and B. E. Anderson, “Time reversal in a phononic crystal using finite-element modeling and an equivalent circuit model,” *JASA Express Lett.* **2**(12), 124002 (2022).
- ⁴⁹E. D. Golightly, B. E. Anderson, A. D. Kingsley, R. Russell, and R. Higgins, “Super resolution, time reversal focusing using path diverting properties of scatterers,” *Appl. Acoust.* **206**, 109308 (2023).
- ⁵⁰M. Tanter, J. Thomas, and M. Fink, “Time reversal and the inverse filter,” *J. Acoust. Soc. Am.* **108**(1), 223–234 (2000).
- ⁵¹K. F. Warnick, “MIMO communications and inverse scattering,” in *2009 IEEE Antennas and Propagation Society International Symposium*, North Charleston, SC (IEEE, Piscataway, NJ, 2009), pp. 1–4.
- ⁵²C. Prada and M. Fink, “Eigenmodes of the time reversal operator: A solution to selective focusing in multiple-target media,” *Wave Motion* **20**, 151–163 (1994).
- ⁵³C. Prada and J.-L. Thomas, “Experimental subwavelength localization of scatterers by decomposition of the time reversal operator interpreted as a covariance matrix,” *J. Acoust. Soc. Am.* **114**, 235–243 (2003).
- ⁵⁴B. Orazbayev and R. Fleury, “Far-field subwavelength acoustic imaging by deep learning,” *Phys. Rev. X* **10**, 031029 (2020).
- ⁵⁵A. Maznev, G. Gu, S.-y. Sun, J. Xu, Y. Shen, N. X. Fang, and S.-y. Zhang, “Extraordinary focusing of sound above a soda can array without time reversal,” *New J. Phys.* **17**(4), 042001 (2015).
- ⁵⁶B. D. Patchett, B. E. Anderson, and A. D. Kingsley, “The impact of room location on time reversal focusing amplitudes,” *J. Acoust. Soc. Am.* **150**(2), 1424–1433 (2021).
- ⁵⁷A. D. Kingsley, J. M. Clift, B. E. Anderson, J. E. Ellsworth, T. J. Ulrich, and P.-Y. L. Bas, “Development of software for performing acoustic time reversal with multiple inputs and outputs,” *Proc. Mtgs. Acoust.* **46**, 055003 (2022).
- ⁵⁸C. Prada, F. Wu, and M. Fink, “The iterative time reversal mirror: A solution to self-focusing in the pulse-echo mode,” *J. Acoust. Soc. Am.* **90**(2), 1119–1129 (1991).
- ⁵⁹C. Prada, J.-L. Thomas, and M. Fink, “The iterative time reversal process: Analysis of the convergence,” *J. Acoust. Soc. Am.* **97**(1), 62–71 (1995).
- ⁶⁰G. Montaldo, M. Tanter, and M. Fink, “Real time inverse filter focusing through iterative time reversal,” *J. Acoust. Soc. Am.* **115**(2), 768–775 (2004).
- ⁶¹I. E. Psarobas, A. Modinos, R. Sainidou, and N. Stefanou, “Acoustic properties of colloidal crystals,” *Phys. Rev. B* **65**, 064307 (2002).
- ⁶²R. S. Penciu, H. Kriegs, G. Petekidis, G. Fytas, and E. N. Economou, “Phonons in colloidal systems,” *J. Chem. Phys.* **118**(11), 5224–5240 (2003).
- ⁶³V. Leroy, A. Strybulevych, M. G. Scanlon, and J. H. Page, “Transmission of ultrasound through a single layer of bubbles,” *Eur. Phys. J. E* **29**, 123–130 (2009).
- ⁶⁴M. L. Cowan, J. H. Page, and P. Sheng, “Ultrasonic wave transport in a system of disordered resonant scatterers: Propagating resonant modes and hybridization gaps,” *Phys. Rev. B* **84**, 094305 (2011).
- ⁶⁵F. Lemoult, N. Kaina, M. Fink, and G. Lerosey, “Wave propagation control at the deep subwavelength scale in metamaterials,” *Nat. Phys.* **9**, 55–60 (2013).
- ⁶⁶F. Lemoult, N. Kaina, M. Fink, and G. Lerosey, “Soda cans metamaterial: A subwavelength-scaled phononic crystal,” *Crystals* **6**(7), 82 (2016).